ROZPRAWY INŻYNIERSKIE • ENGINEERING TRANSACTIONS • 29, 1, 131–142, 1981
Polska Akademia Nauk • Instytut Podstawowych Problemów Techniki

TRANSIENT NONLINEAR RESPONSE OF IMPULSIVELY-LOADED CIRCULAR PLATES

M. T. E. TUOMALA and M. J. MIKKOLA (ESPOO)

The finite element procedure used in this study is based on the incremental Lagrangian approach. Geometrical nonlinearity is included. The elastic viscoplastic material model is adopted in a form suitable for large strains. Linear 2-noded and parabolic 3-noded isoparametric axisymmetric shell elements are employed. Numerical time integration is carried out by the central difference scheme. The agreement between computed and experimental results is at least satisfactory. The discrepancies can be explained by combined effects of small inaccuracies of loading geometry, constitutive parameters, boundary conditions, and numerical discretization and round-off errors

1. Introduction

Research on the dynamic plastic response of structures has been widely reviewed in Ref. [1]. Circular plates under impulsive loading have received considerable, attention, see Ref. [2–18]. Experimental results have been reported in Ref. [7, 9, 10, 14], and various analytical and numerical techniques have been applied, see Ref. [12, 13, 15, 16] — the mode approximation technique, Ref. [9] — the finite difference method, and Ref. [17, 18] — the finite element method.

A comprehensive experimental investigation is described by BODNER and SYMONDS [14]. Circular plates, made of mild steel and titanium, were clamped in a manner intended to prevent displacements in the plane of the plate as well as transverse displacements and slopes. The transverse pulse loading on the plate was applied by detonating a disk of explosive sheet separated from the plate by a styrofoam buffer pad of the same radius and 1/4 in. thickness. Three loading geometries were used, $a/R=1$, 1/2, and 1/3. a/R was the ratio of the loaded area radius to the plate radius. The primary measurement in each test were the initial impulse imparted to the specimen, the final mid-point deflection and the deflection profile. Approximate measurements were also made of deflection time history, furnishing information about times of reaching peak or final deflection magnitudes.

The purpose of this paper is to report on the finite element computations which were made on some specimens tested by Bodner and Symonds. Besides the overall performance of the finite element procedure, which was studied by comparison of the computed and experimental results, the effects of strain hardening and strain rate behaviour of the viscoplastic material model, the influence of the change in loading geometry, and the effect of partial fixing of the plate edge were investigated.

The finite element procedure used in this study is based on the updated or incremental Lagrangian approach. Geometrical nonlinearity is included. The elastic viscoplastic material model is adopted in a form suitable for large strains. Linear 2-noded and parabolic 3-noded isoparametric axisymmetric shell elements are employed. Numerical time integration is carried out by the central difference method.

2. Equations of equilibrium

Consider the motion of a body in a Cartesian coordinate system. In the Lagrangian approach the principle of virtual work can be expressed in the form [19]

$$\int_V S_{ij}\,\delta E_{ij}\,dV+\int_V \rho\ddot{u}_i\,\delta u_i\,dV=\int_V b_i\,\delta u_i\,dV+\int_{S_t} t_i\,\delta u_i\,dS, \tag{2.1}$$

where V and S are the volume and the surface of the body in the reference configuration, respectively, S_{ij} is the 2nd Piola–Kirchhoff stress tensor, ρ the mass density, u_i and $\ddot{u}_i$ the displacement and acceleration vectors, respectively, b_i the body force per unit volume, t_i the surface load, and E_{ij} the Green–Lagrange strain tensor

$$E_{ij}=(u_{i,j}+u_{j,i}+u_{k,i}\,u_{k,j})/2. \tag{2.2}$$

In the finite element method, the principle of virtual work (2.1) results in the matrix equation (see e.g. [20])

$$R(q)+M\ddot{q}=Q, \tag{2.3}$$

where q is the vector of nodal displacements and

$$R=\int_V B^T S\,dV, \quad Q=\int_V N^T b\,dV+\int_{S_t} N^T t\,dS, \quad M=\int_V N^T \rho N\,dV \tag{2.4}$$

the vector of internal forces, the vector of external loads, and the mass matrix, respectively. N is the matrix of shape functions in the definition of the displacement field $u=Nq$, and the matrix B, dependent on the current configuration, is defined by the strain variation

$$\delta E=B\delta q. \tag{2.5}$$

In the total Lagrangian approach, a fixed reference configuration, usually the initial configuration, is used. In the updated or incremental Lagrangian approach, the current configuration is chosen as the reference configuration. A mixed approach is obtained by changing the reference configuration after a certain number of time or load steps.

3. Constitutive equations

It is assumed that the strain rate can be decomposed into elastic and viscoplastic parts

$$D_{ij}=D^e_{ij}+D^{vp}_{ij}. \tag{3.1}$$

The Jaumann rate of Euler stress

$$\overset{*}{T}_{ij}=\dot{T}_{ij}-W_{ik}\,T_{kj}-W_{jk}\,T_{ik} \tag{3.2}$$

and the elastic part of strain rate are related by Hooke's law (see [22])

$$\overset{*}{T}_{ij}=(E/1+\nu)\,[(\delta_{ik}\,\delta_{jl}+\delta_{il}\,\delta_{jk})/2+\delta_{ij}\,\delta_{kl}\,\nu/(1-2\nu)]\,D^{e}_{kl}=C_{ijkl}\,D^{e}_{kl}. \tag{3.3}$$

$\dot{T}_{ij}$ is the material rate of Euler stress and W_{ij} the spin tensor

$$W_{ij}=(\partial v_i/\partial y_j-\partial v_j/\partial y_i)/2, \tag{3.4}$$

v is the velocity and y the spatial Cartesian coordinate system. The viscoplastic part of strain rate obeys the associated flow rule of viscoplasticity [21]

$$D^{vp}_{ij}=\gamma\,\langle\Phi\,(F)\rangle\,\frac{\partial f}{\partial T_{ij}}, \tag{3.5}$$

where γ is a viscosity coefficient, $F\equiv f/\sigma_y-1$, Φ an appropriately chosen function (the power function $\Phi\,(F)=\text{sign}\,(F)\,|F|^{p}$ was used), and the notation $\langle\ \rangle$ means that $\langle x\rangle=x$ when $x>0$ and $\langle x\rangle=0$ when $x\leqslant 0$. The Huber-Mises yield condition

$$f-\sigma_y=0 \tag{3.6}$$

is expressed in terms of Euler stress

$$f=\sqrt{3\bar{T}_{ij}\,\bar{T}_{ij}/2}, \qquad \bar{T}_{ij}=T_{ij}-\delta_{ij}\,T_{kk}/3. \tag{3.7}$$

On the basis of Eqs. (3.1) and (3.3) the Jaumann rate of Euler stress is

$$\overset{*}{T}_{ij}=C_{ijkl}\,(D_{kl}-D^{vp}_{kl}) \tag{3.8}$$

with

$$D^{vp}_{kl}=3\gamma\,\langle\Phi\,(F)\rangle\,\bar{T}_{kl}/2f. \tag{3.9}$$

In the step-by-step solution, the increment of the 2nd Piola-Kirchhoff stress ΔS is needed. The general transformation rule between the Piola-Kirchhoff stress and the Cauchy stress is

$$S=JG^{-1}\,T\,(G^{-1})^{T}, \tag{3.10}$$

where G is the deformation gradient and J the Jacobian of the deformation gradient. Differentiation with respect to time yields

$$\dot{S}=JG^{-1}\,(\dot{T}-LT-TL^{T}+trLT)\,(G^{-1})^{T}, \tag{3.11}$$

where $L=\dot{G}G^{-1}$ is the velocity gradient. Observing that $L=D+W$ and Eq. (3.2), one obtains

$$\dot{S}=JG^{-1}\,(\overset{*}{T}-DT-TD^{T}+trDT)\,(G^{-1})^{T}. \tag{3.12}$$

In the incremental Lagrangian formulation, the stress quantities S and T coincide at the beginning of the step, and $G=I$ and $J=1$. The formula (3.12) yields thus

$$\dot{S}_{ij}=C_{ijkl}\,(D_{kl}-D^{vp}_{kl})-T_{ik}\,D_{jk}-T_{kj}\,D_{ik}+D_{kk}\,T_{ij}, \tag{3.13}$$

where the relationship (3.8) has been taken into account. The increment of S_{ij} is approximately

$$\Delta S_{ij}=\dot{S}_{ij}\,\Delta t \tag{3.14}$$

and the new value of stress $S_{ij}(t+\Delta t)=S_{ij}(t)+\Delta S_{ij}$. The Euler stress in the new reference configuration at the instant $t+\Delta t$ is found through transformation:

$$T=J^{-1}\,GS\,(t+\Delta t)\,G^T, \tag{3.15}$$

where G is the deformation gradient corresponding to the displacement increments Δu, $G_{ij}=\partial\,(y_i+\Delta u_i)/\partial y_j$, and J the Jacobian of this deformation gradient.

The true yield stress σ_y is a function of the logarithmic plastic strain

$$\bar{\varepsilon}^p=\int \sqrt{2D_{ij}^{vp}\,D_{ij}^{vp}/3}\,dt. \tag{3.16}$$

The relationship $\sigma_y=\sigma_y(\bar{\varepsilon}^p)$ can be found from uniaxial tensile test, in which case the tensile stress σ equals σ_y and D_{11}^{vp} equals $\dot{\bar{\varepsilon}}^p$.

4. Solution technique

The spatially discretized equation (2.3) is a set of ordinary differential equations with respect to time. Various time integration algorithms for the solution of this equation have been used and their merits discussed in papers on structural dynamics. In this study the central difference method (*CD*) was employed. In the *CD* scheme the solution q_{n+1} at time t_{n+1} is computed from the formula

$$q_{n+1}=h^2\,M^{-1}\,(Q_n-R_n)+2q_n-q_{n-1}, \tag{4.1}$$

where $h=t_{n+1}-t_n$ is the step length. The strain increment is

$$\Delta E=B_n\,(q_{n+1}-q_n)\approx D_n\,h\,. \tag{4.2}$$

The stress increment ΔS can be computed in accordance with the formulae (3.13) and (3.14). After the necessary transformations for the new reference configuration, the next time step can be taken. The initial condition for $q_0=(q_1-q_{-1})/2h$ has to be used to eliminate q_{-1} in the first step. Computing effort is much reduced when the diagonal mass matrix is employed. The *CD* scheme is accurate and simple. As an explicit difference method, its step length is limited by the largest natural frequency of the finite element mesh.

5. Isoparametric axisymmetric shell element

The geometry of the axisymmetric element is defined in a Cartesian coordinate system, where x is the radial direction and y is the rotation axis, by the transformation [18]

$$\begin{aligned} x(\xi,\eta)&=\sum_1^n N_i(\xi)\,x_i+\eta\sum_1^n \frac{1}{2}h_i N_i(\xi)\cos\alpha_i,\\ y(\xi,\eta)&=\sum_1^n N_i(\xi)\,y_i+\eta\sum_1^n \frac{1}{2}h_i N_i(\xi)\sin\alpha_i, \end{aligned} \tag{5.1}$$

in which x_i, y_i are the nodal point coordinates, h_i the shell thickness, $\xi, \eta \in (-1, 1)$ are curvilinear coordinates such that ξ is along the shell midsurface and the η-axis is along the surface $\xi=0$, α_i is the angle between the x- and η-axes at nodal point i, $N_i(\xi)$ are shape functions (Fig. 1). The displacement increments are

$$\Delta u(\xi,\eta)=\Sigma N_i(\xi)\,\Delta u_i+\eta\Sigma\frac{1}{2}h_i N_i(\xi)(-\sin\alpha_i)\,\Delta\varphi_i,$$

(5.2)

$$\Delta v(\xi,\eta)=\Sigma N_i(\xi)\,\Delta v_i+\eta\Sigma\frac{1}{2}h_i N_i(\xi)\cos\alpha_i\,\Delta\varphi_i,$$

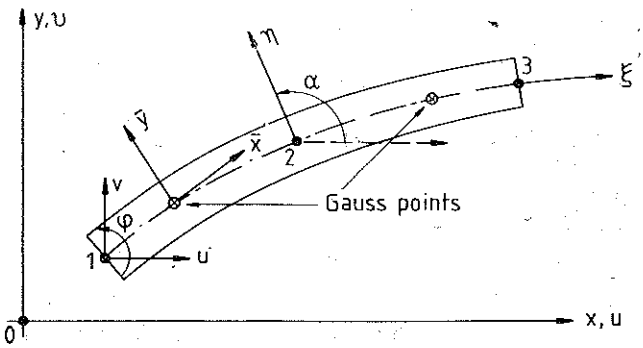

FIG. 1. Coordinate system for the isoparametric axisymmetric shell element.

where Δu_i. Δv_i are the nodal point displacement increments and $\Delta\varphi_i$ the nodal point rotation increment. The displacement increments are transformed to a local $\bar{x}$, $\bar{y}$ coordinate system, where $\bar{x}$ is tangent and $\bar{y}$ normal to the midsurface (Fig. 1). The strains are in the local coordinate system

$$\Delta\varepsilon_{\bar{x}}=\Delta\bar{u}_{,\bar{x}}+(\Delta\bar{u}_{,\bar{x}})^2/2+(\Delta\bar{v}_{,\bar{x}})^2/2,$$

(5.3)

$$\Delta\gamma_{\bar{x}\bar{y}}=\Delta\bar{u}_{,\bar{y}}+\Delta\bar{v}_{,\bar{x}}+\Delta\bar{u}_{,\bar{x}}\,\Delta\bar{u}_{,\bar{y}},$$

$$\Delta\varepsilon_\theta=\Delta u/x+(\Delta u/x)^2/2.$$

The strain variation $\delta\Delta\varepsilon=B\delta q$ produces the matrix B. The stress increments are also evaluated in the local frame. The new nodal point coordinates are $x_i(t+\Delta t)=x_i(t)+\Delta u_i$ etc.

A linear Lagrangian shape function $N_i(\xi)$ leads to a 6 degree of freedom element while a parabolic shape function gives 9 degrees of freedom. The integration in the ξ variable is carried out by a one point Gaussian for the linear and by a two point Gaussian rule for the parabolic element. Simpson's rule is adopted for the thickness direction.

6. NUMERICAL EXAMPLES

Data of the test plates of Bodner and Symonds [14] is given in Table 1 below. The materials were hot rolled mild steel (ASTM A415) and 99.2% pure titanium (Ti–50A), which are both strongly strain-rate sensitive materials. For mode approx-

imation calculations Bodner and Symonds assumed that the results of upiaxial stress tests can be expressed by the equation

$$\sigma/\sigma_0 = 1 + (\dot{\varepsilon}/\dot{\varepsilon}_0)^{1/p}, \tag{6.1}$$

Table 1.

	steel	titanium
Mass density ρ [$lb\,s^2/in^4$]	0.73×10^{-3}	0.42×10^{-3}
Plate radius R [in]	1.25	1.25
Plate thickness (average) H [in]	0.076	0.092
Strain-rate constant σ_0 [psi]	32400	36400 at $\varepsilon^p=1\%$ 38500 at $\varepsilon^p=2\%$
Strain-rate constant $\dot{\varepsilon}_0$ [1/s]	40	120
Strain-rate constant p	5	9
Modulus of elasticity E [psi]	30×10^6	17×10^6
Tangent modulus E_T [psi]	8.33×10^4	1.4×10^5
Initial yield stress σ_{y0} [psi]	35000	40000

where σ and $\dot{\varepsilon}$ are the tensile (compressive) stress and the strain rate, respectively, and σ_0, $\dot{\varepsilon}_0$, and p are material constants. The parameter ε_0 corresponds to the viscosity coefficient γ in Eq. (3.5) and p is the exponent of the yield function F. Two strain hardening models were used in the finite element computations: one elastic, ideally plastic, and the other elastic, linearly hardening (bilinear). The moduli E and E_T are shown in Table 1 where the initial yield stress σ_{y0} of the bilinear relationship

$$\sigma_y = \sigma_{y0} + E_p\,\bar{\varepsilon}^p, \qquad E_p = E_T\,E/(E-E_T) \tag{6.2}$$

is also given. The shape of the load pulse was assumed to be triangular with the rise time of 5 μs and the total duration of 10 μs.

The final central deflections from 24 computer runs are shown in Figs. 2–5. Finite element solutions were computed for steel specimens No. 46, 57, 59 with ratio $a/R=1$, and No. 64, 65 with $a/R=1/2$, and for titanium specimens No. 79, 94 with $a/R=1$, and No. 71, 74, 77 with $a/R=1/2$. Ten linear isoparametric shell elements were employed. Numerical time integration was performed using the central difference scheme with time step $\Delta t=0.25$ μs. As a rule, the finite element results agree satisfactorily with the experimental and theoretical values by the node approximation method. Inclusion of the strain-hardening effect does not consistently improve the agreement. To investigate the influence of loading geometry, the case $a/R=0.5$ was also computed using the value $a/R=0.6$. For titanium plate this gave a closer fit with the experimental values. In Fig. 6 the form of the permanent deflection of the titanium plate specimen No. 74 is depicted. The computed result of a strain hardening model with $a/R=0.6$ is fairly close to the measured form.

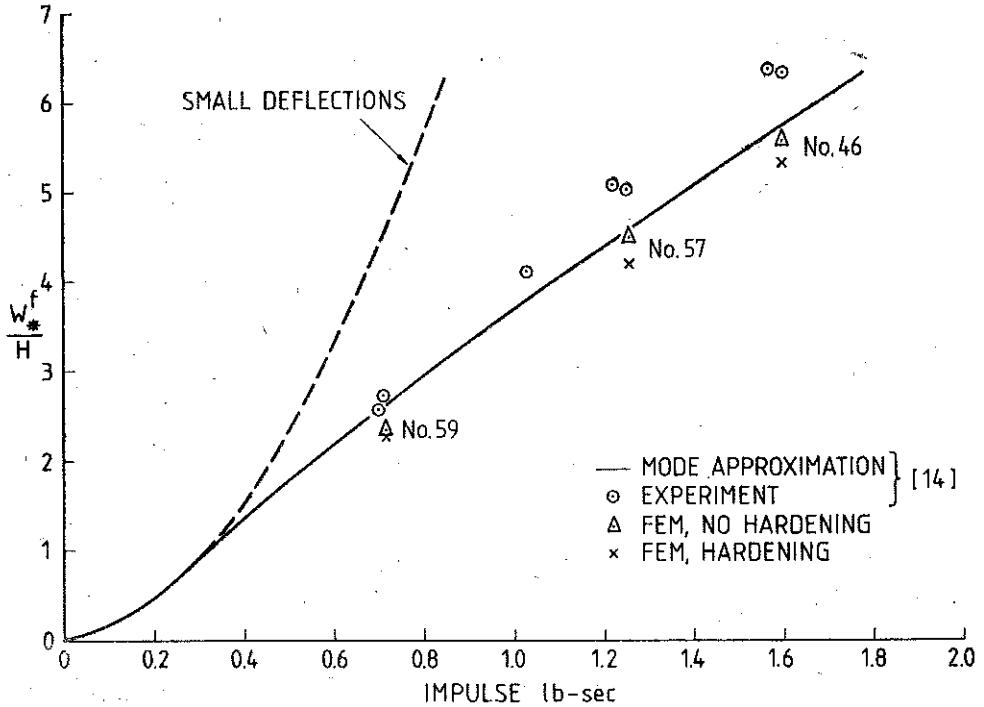

FIG. 2. Final midpoint deflection vs impulse for steel plates with $a/R=1$.

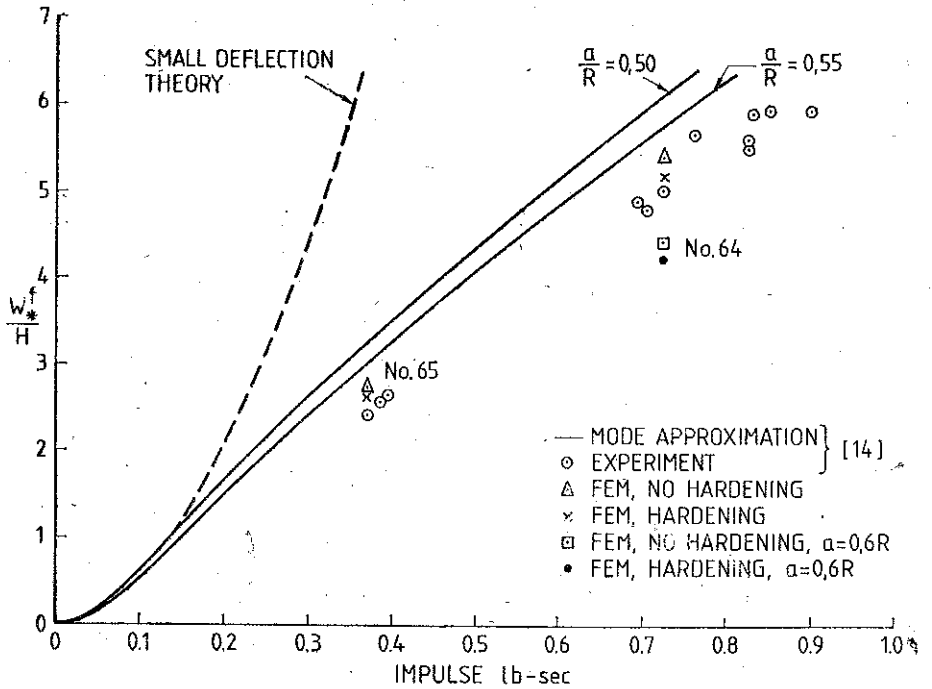

FIG. 3. Final midpoint deflection vs impulse for steel plates with $a/R=0.5$.

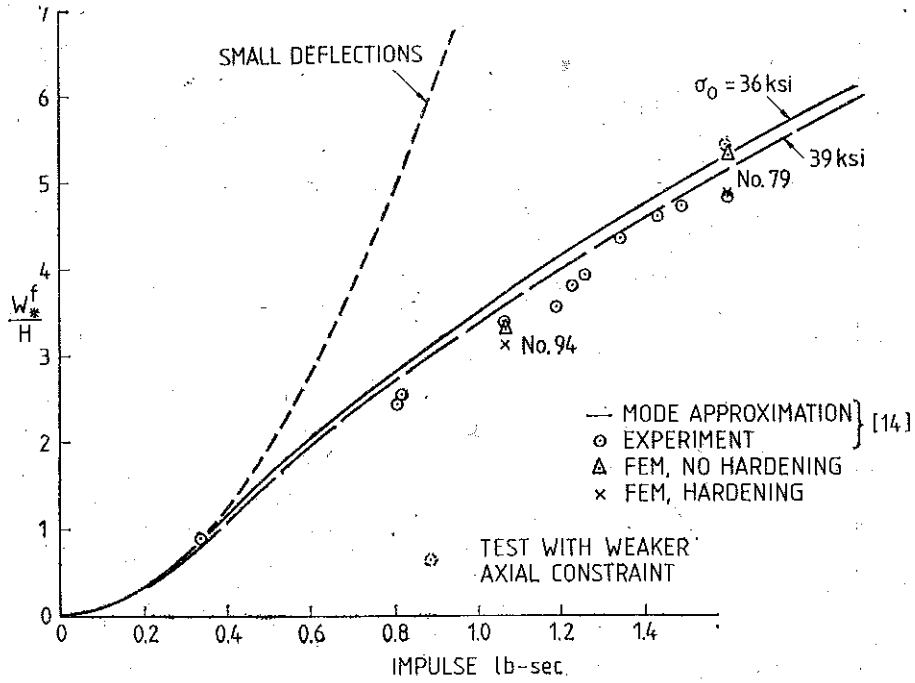

FIG. 4. Final midpoint deflection vs impulse for titanium plates with $a/R=1$.

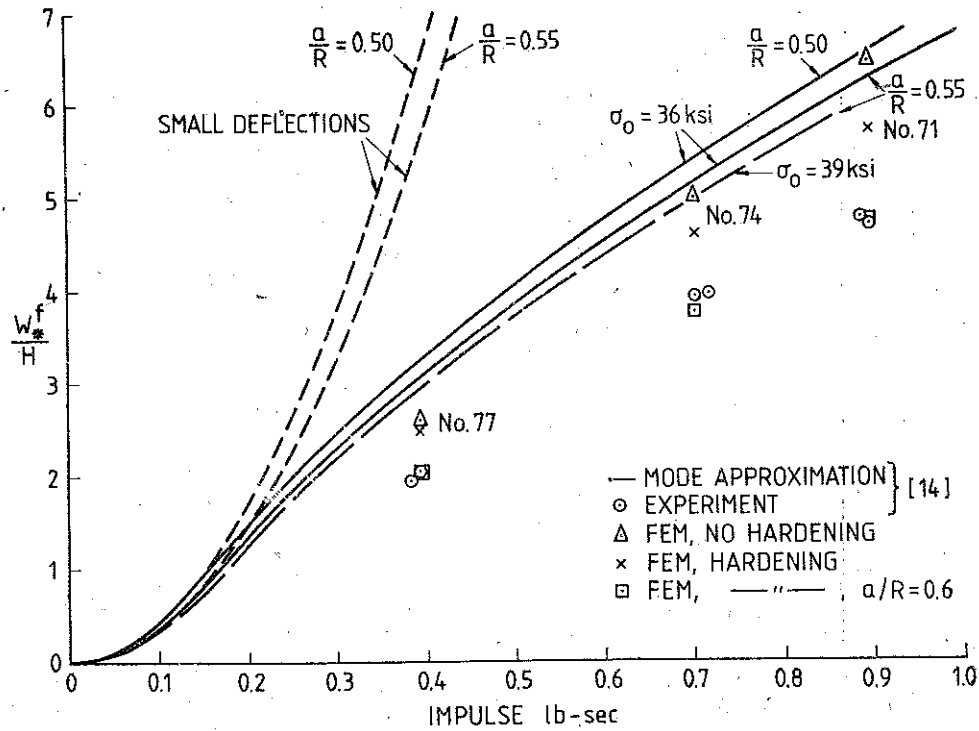

FIG. 5. Final midpoint deflection vs impulse for titanium plates with $a/R=0.5$.

In Fig. 7 the convergence of the central deflection vs time for steel plate specimen No. 57 is illustrated. In the case of 10 parabolic isoparametric elements the time step $\Delta t=0.25\,\mu s$ was used, while for 10 linear isoparametric elements the time step was $\Delta t=2.5\,\mu s$ and for 20 linear isoparametric elements $\Delta t=1.25\,\mu s$. The conformity of the computed curves is very good.

The effect of the strain-rate dependency was investigated by comparing two viscoplasticity functions. The power function $\dot{\varepsilon}^p=40\,s^{-1}(\sigma/\sigma_y-1)^5$ corresponds to Manjoine's test results for steel. The expression $\dot{\varepsilon}^p=\Sigma B_\alpha(\sigma/\sigma_y-1)^\alpha$ was adapted to the test result by Clark and Duwez. The values of the constants B_α can be found in Ref. [21] p. 287, the formula (2.92b), Table 2, line 2. The more complex expression

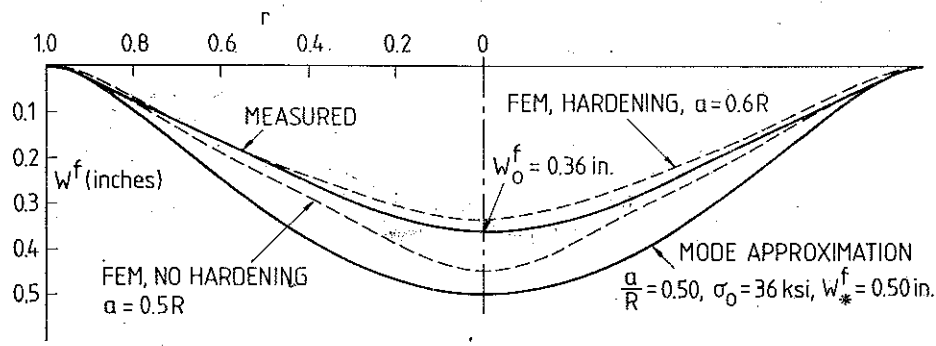

FIG. 6. Final deflection profile of titanium plate specimen No. 74, $a/R=0.5$.

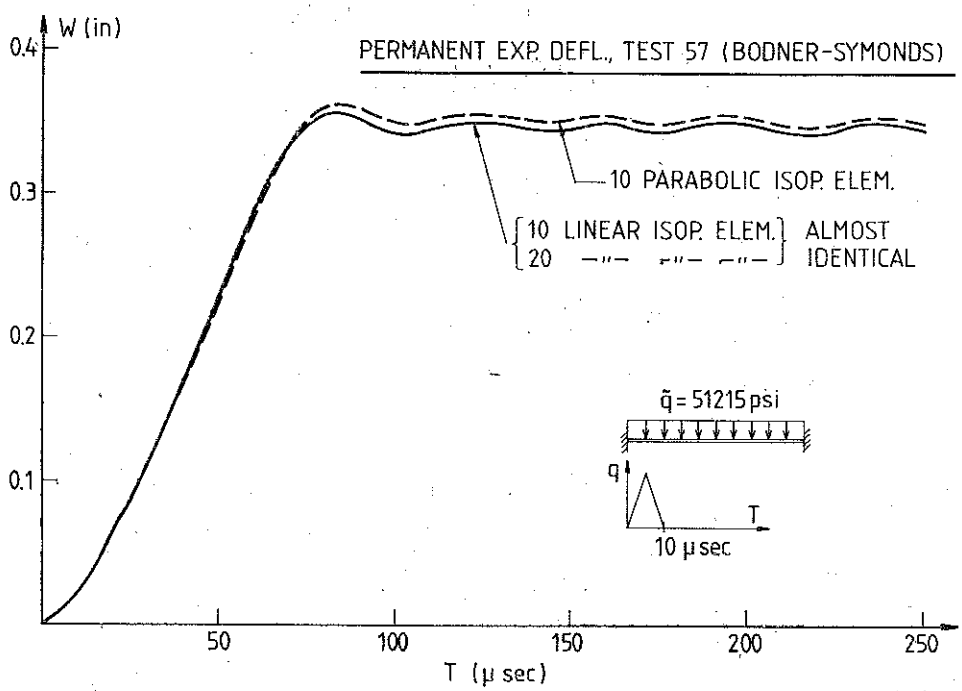

FIG. 7. Midpoint deflection vs time of steel plate specimen No. 57, $a/R=1$. No strain hardening.

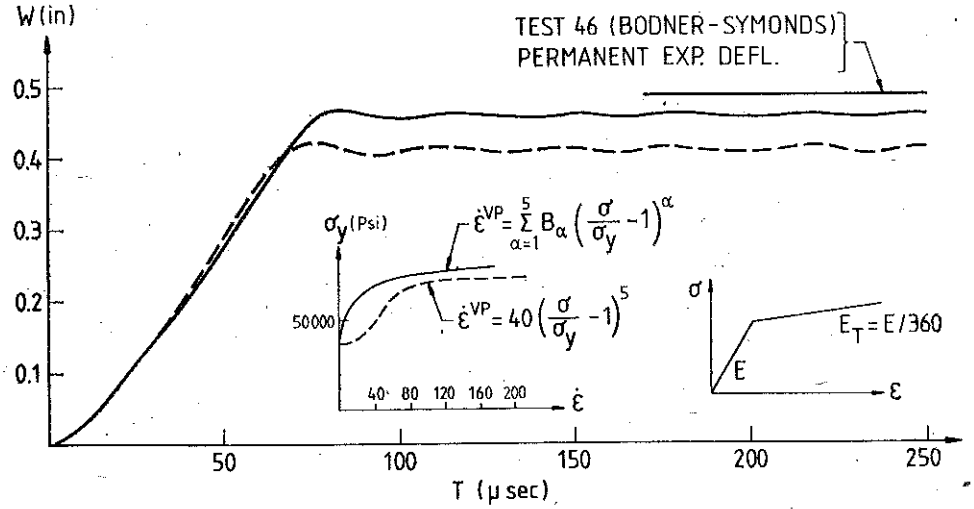

FIG. 8. Midpoint deflection vs time of steel plate specimen No. 46, $a/R=1$. Comparison of two viscoplasticity functions.

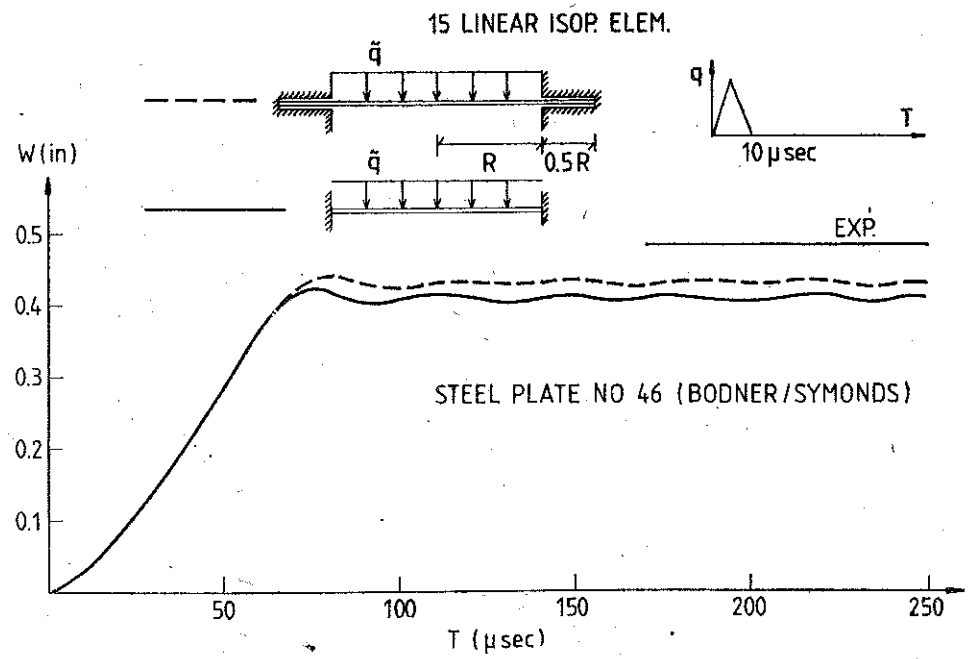

FIG. 9. Midpoint deflection vs time of steel plate specimen No. 46, $a/R=1$. Effect of partial failure of the in-plane fixing.

provides closer agreement with the experimental deflection of steel plate specimen No. 46 (Fig. 8).

BODNER and SYMONDS [14] remarked that the clamping mechanism did not fully prevent inward displacements at the largest load magnitudes. The inward displacements at the plate edge were generally less than 1/16 in (1.6 mm). Computationally, the effect of inward in-plane displacements was studied by modifying the boundary conditions. One solution was computed by assuming completely rigid clamping at the boundary. For the other solution, clamping against rotation at the plate edge was assumed but the clamping against in-plane displacement was at a distance $0.5\,R$ from the edge. The in-plane movement was assumed to take place without friction. This boundary condition was considered to simulate the partial failure of the fixing observed at tests. The results in Fig. 9 indicate that the effect of inward displacement, although in the right direction, does not wholly explain the discrepancy between numerical and experimental results.

7. CONCLUSIONS

The comparisons between computed and experimental results indicate that the numerical procedure is capable to predict the behaviour of plates subjected to impulsive loadings. The discrepancies between computed and test results can be due to the combined effects of small inaccuracies of loading geometry, constitutive parameters, boundary conditions, and numerical discretization and round-off errors.

REFERENCES

1. N. JONES, *A literature review of the dynamic plastic response of structures*, The Shock and Vibration Digest, **7**, 89–105, 1975.
2. A. J. WANG, H. G. HOPKINS, *On the plastic deformation of built-in circular plates under impulsive load*, J. Mech. Phys. Solids, **3**, 22–37, 1954.
3. A. J. WANG, *The permanent deflection of a plastic plate under blast loading*, J. Appl. Mech., **22**, 375–376, 1955.
4. T. WIERZBICKI, *Dynamics of rigid viscoplastic circular plates*, Arch. Mech., **17**, 6, 851–869, 1965.
5. T. WIERZBICKI, *Impulsive loading of rigid viscoplastic plates*, Int. J. Solids Struct., **3**, 4, 635–647, 1967.
6. A. L. FLORENCE, *Clamped circular rigid-plastic plates under blast loading*, J. Appl. Mech., **33**, 256–260, 1966.
7. A. L. FLORENCE, *Circular plates under a uniformly distributed impulse*, Int. J. Solids Struct., **2**, 37–47, 1966.
8. N. JONES, *Impulsive loading of a simply supported circular rigid plastic plate*, J. Appl. Mech., **35**, 59–65, 1968.
9. T. A. DUFFEY, S. W. KEY, *Experimental-theoretical correlations of impulsively loaded clamped circular plates*, Exp. Mech., **9**, 241–249, 1969.
10. T. WIERZBICKI, A. L. FLORENCE, *A theoretical and experimental investigation of impulsively loaded clamped circular viscoplastic plates*, Int. J. Solids Struct., **6**, 553–568, 1970.
11. R. C. BATRA, R. N. DUBEY, *Impulsively loaded circular plates*, Int. J. Solids Struct., **7**, 965–978, 1971.
12. C. T. CHON, P. S. SYMONDS, *Large dynamic deflection of plates by mode method*, J. Eng. Mech. Div., Proc. ASCE 103, EM1, 3–14, 1977.

1 P. S. SYMONDS, C. T. CHON, *On dynamic mode-form solutions*, J. Mech. Pys. Solids, **26**, 21–35, 1978.
14. S. R. BODNER, P. S. SYMONDS, *Experiments on viscoplastic response of circular plates to impulsive loading*, Tech. Report NOOO14-0860/6, Brown Univ., Providence, R. I., July 1977.
15. P. S. SYMONDS, C. T. CHON, *Finite viscoplastic deflections of an impulsively loaded plate by the mode approximation technique*, Tech. Report NOOO14-0860/5, Brown Univ., Providence, R. I., September 1977.
16. P. S. SYMONDS, T. WIERZBICKI, *Membrane mode solutions for impulsively loaded circular plates*, Tech. Report ENG77-11877/1, Brown Univ., Providence, R. I., July 1978.
17. T. BELYTSCHKO, B. J. HSIEH, *Nonlinear transient analysis of shells and solids of revolution by convected elements*, AIAA J., **12**, 8, 1031–1035, 1974.
18. M. T. E. TUOMALA, M. J. MIKKOLA, *Transient dynamic large deflection analysis of elastic viscoplastic plates by the finite element method*, Int. J. Mech. Sci., **22**, 3, 151–166, 1980,
19. K. WASHIZU, *Variational methods in elasticity and plasticity*, Pergamon Press, 2nd edition, Oxford 1975.
20. O. C. ZIENKIEWICZ, *The finite element method*, McGraw-Hill, 3rd edition, London 1977.
21. P. PERZYNA, *Fundamental problems in viscoplasticity*, Advances in Applied Mechanics, **9**, 243–377, 1966.
22. R. M. MCMEEKING, J. R. RICE, *Finite-element formulations for problems of large elastic-plastic deformation*, Int. J. Solids Struct., **11**, 5, 601–616, 1975.

STRESZCZENIE

NIELINIOWA ANALIZA NUMERYCZNA IMPULSOWO OBCIĄŻONEJ PŁYTY KOŁOWEJ

Zastosowana w pracy metoda elementów skończonych oparta jest na przyrostowym podejściu Lagrange'a. Uwzględnione są geometryczne nieliniowości. Przyjęto równania konstytutywne dla materiału sprężysto-lepkoplastycznego dla dużych odkształceń. Zastosowano izometryczny liniowy element powłokowy z dwoma węzłami oraz paraboliczny z trzema węzłami. Całkowanie względem czasu przeprowadzono jest za pomocą schematu różnicowego centralnego. Zgodność uzyskanych wyników z rezultatami eksperymentu jest co najmniej zadowalająca. Zaobserwowane różnice mogą być wyjaśnione przez łączne efekty niedokładności w warunkach obciążenia, warunkach brzegowych, parametrach konstytutywnych oraz w błędach zaokrągleń i dyskretyzacji.

Резюме

НЕЛИНЕЙНЫЙ ЧИСЛЕННЫЙ АНАЛИЗ КРУГОВОЙ ПЛИТЫ НАГРУЖЕННОЙ ИМПУЛЬСНЫМ ОБРАЗОМ

Примененный в работе метод конечных элементов опирается на подход Лагранжа в приростах. Учтены геометрические нелинейности. Приняты определяющие уравнения для упруго-вязкопластического материала для больших деформаций. Применены изометрический элемент с тремя узлами. Интегрирование по времени проведено при помощи разностной центральной схемы. Совпадение полученных результатов с результатами эксперимента по крайней мере удовлетворительно. Наблюдаемые разницы могут быть выяснены совместными эффектами неточностей в условиях нагружения в граничных условиях в определяющих параметрах а также в ошибках округлений и дискретизации.

DEPARTMENT OF CIVIL ENGINEERING
HELSINKI UNIVERSITY OF TECHNOLOGY

Received March 20, 1980.